Chemistry & Biology 13, 201–211, February 2006 ©2006 Elsevier Ltd All rights reserved DOI 10.1016/j.chembiol.2005.11.011

Differential Binding of Inhibitors to Active and Inactive CDK2 Provides Insights for Drug Design

George Kontopidis,[1,4,*] Campbell McInnes,[1,4] Sravan R. Pandalaneni,[1,3] Iain McNae,[2] Darren Gibson,[1] Mokdad Mezna,[1] Mark Thomas,[1] Gavin Wood,[1] Shudong Wang,[1] Malcolm D. Walkinshaw,[1,2] and Peter M. Fischer[1]

[1] Cyclacel Ltd.
James Lindsay Place
Dundee, DD1 5JJ
United Kingdom

[2] Structural Biochemistry
The University of Edinburgh
Michael Swann Building
King's Buildings
Edinburgh, EH9 3JR
United Kingdom

[3] University of Abertay
Dundee, DD1 1HG
United Kingdom

Summary

The cyclin-dependent kinases (CDKs) have been characterized in complex with a variety of inhibitors, but the majority of structures solved are in the inactive form. We have solved the structures of six inhibitors in both the monomeric CDK2 and binary CDK2/cyclinA complexes and demonstrate that significant differences in ligand binding occur depending on the activation state. The binding mode of two ligands in particular varies substantially in active and inactive CDK2. Furthermore, energetic analysis of CDK2/cyclin/inhibitors demonstrates that a good correlation exists between the in vitro potency and the calculated energies of interaction, but no such relationship exists for CDK2/inhibitor structures. These results confirm that monomeric CDK2 ligand complexes do not fully reflect active conformations, revealing significant implications for inhibitor design while also suggesting that the monomeric CDK2 conformation can be selectively inhibited.

Introduction

CDKs fulfill numerous and partly overlapping functions in the regulation of both the cell proliferation cycle and the RNA polymerase-II (RNAP-II) transcription cycle [1]. However, the demonstration that CDK2 activity appears to be redundant for the proliferation of normal cells [2], and in some cases of cancer cells [3], has led to questions regarding the validity of CDK2 as a drug target for proliferative diseases [4, 5]. Nevertheless, the potential of pharmacological CDK2 inhibition in suppressing cell proliferation remains to be explored. At present, appropriate mechanistic questions are difficult to answer because small-molecule inhibitors invariably also suppress CDKs other than CDK2, especially CDK1, which regulates entry into mitosis, as well as CDK7 and CDK9 [6].

The latter two CDKs have been implicated in the regulation of RNAP-II activation in addition to their cell cycle-related functions [7–9]. The expression of many genes is regulated at the level of RNA transcription, and CDK7 and CDK9 form part of the general transcription factors TFIIH and p-TEFb, respectively, in which they activate RNAP-II through phosphorylation of its C-terminal domain (CTD). Other members of the CDK family, including CDK1, CDK8, and especially CDK2, that were originally ascribed cell cycle functions only, are now known to participate in the regulation of RNAP-II[10]. Transformed cells require continuous activity of RNAP-II to resist oncogene-induced apoptosis [11], and a new oncology CDK target rationale based on inhibition of transcription has been proposed [12].

Despite the complexities of their mechanism of action, CDKs remain the focus of intense efforts in drug development. Several inhibitors with activity against CDKs are currently under clinical examination in cancer research [13–16].

Here, we shall confine our analysis to CDK2, the best-characterized member of the CDK family in terms of structural biology. It is known that binding of cyclins A and E induces a structural reorganization in CDK2 that is necessary for activation [17, 18]. The reorganization is believed to be a two-step process [19]. First, the PSTAIRE helix of CDK2 is bound between the α3 and α5 helices of cyclin A, followed by additional contacts of cyclin A with the C-terminal lobe of CDK2. Monomeric CDK2 has virtually no activity; however, when phosphorylated, it has been shown to possess about 1% of the activity of the fully active binary complex (16 versus 1600 pmol$\cdot$min$^{-1}\cdot\mu$g^{-1}) [20, 21]. As in many protein kinases, the inactive conformation occurs when, in the absence of posttranslational modification, the catalytic and substrate binding sites are occluded, or inappropriately aligned for phosphotransferase activity [22]. For CDK2, partnering with cyclins A or E results in rotation of the PSTAIRE helix by 45° relative to the monomeric enzyme. While some kinases are catalytically competent in the phosphominus state, an activation step involving phosphorylation of a tyrosine-, serine-, or threonine-containing loop is required in order to produce the activated enzyme. In the CDK2/cyclin A or CDK2/cyclin E complex, the activation loop is relocated from the phosphoacceptor and ATP binding sites to interact with the cyclin, in a movement of approximately 25 Å. Subsequent phosphorylation at T160 by the CDK-activating kinase (CAK; a complex of CDK7, cyclin H, and MAT-1) results in stabilization of the cyclin bound CDK2 structure and generation of the fully active conformation. Together this process results in the formation of a catalytically competent ATP cleft and substrate binding site [23].

CDK2 is one of the best-characterized kinases in structural terms, and there exist approximately 70 X-ray crystal structures of CDK2 inhibitor complexes in the Protein Data Bank (PDB). A wealth of structural data is thus available for analysis and use in the further

*Correspondence: gkontopidis@cyclacel.com
[4] These authors contributed equally to this work.

Table 1. Chemical Structures, In Vitro Inhibition, and Comparison of the Calculated Energetics for CDK2 Inhibitors in Monomeric and Activated Complexes

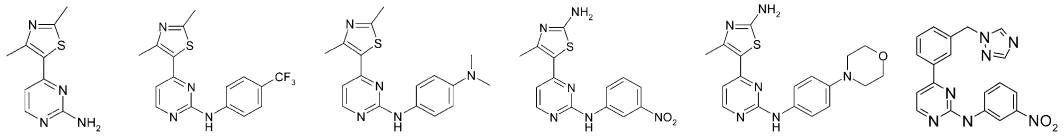

	1		2		3		4		5		6	
	CDK2	CDK2A	CDK2	CDK2A	CDK2	CDK2A	CDK2	CDK2A	CDK2	CDK2A	CDK2	CDK2A
IC_{50} (μM)	6.50	6.50	0.29	0.29	0.22	0.22	0.01	0.01	0.74	0.74	0.25	0.25
NB energy	−45.3	−27.8	−41.1	−60.2	−57.6	−58.1	−37.3	−72.5	−82.0	−40.3	−56.7	−51.6

optimization and development of ATP-competitive compounds [15]. Of these structures, however, only about 20% contain the activated CDK2 kinase state. In addition, the coordinates of only two structures with ATP-competitive ligands, the purine derivative NU2058 [24] and an oxindole derivative [25], were deposited in the PDB as both CDK2 and CDK2/cyclin A complexes. In the latter case, however, different oxindoles were used in the monomeric and activated CDK2 structures. A recent study described a structural comparison with indirubin 5-sulfonate as the ligand in both inactive and active forms of CDK2 [26]. The main conclusions were: (1) the adenine binding site of CDK2 was similar in both forms, and the inhibitor made comparable contacts in this region; (2) residues outside of this region, including residues of the Gly-rich loop and the side chains of K33 and D145, have different positioning, and therefore make different contacts with the ligand, in the monomeric and binary complexes. These conclusions were made on the basis of only one CDK2 ligand, and additional comparisons of these data are not possible, as only the activated kinase inhibitor structure was deposited in the PDB. We have solved six CDK2 ligands based on the previously described 2-anilino-4-(hetero)aryl-pyrimidine pharmacophore [27, 28] in both monomeric and cyclin A bound CDK2 complexes. These structures show that, depending on the size and substitution of the ligand core structure, significantly different inhibitor binding modes are observed in each context. In addition, a detailed study of the existing data from several of the currently available CDK2 structures is presented comparing the energetics of binding and protein/ligand contacts of inhibitors in active and inactive CDK2 conformations. We thus give a comprehensive picture of the structural differences that occur upon ligand binding to both activation states and outline the implications for CDK2 inhibitor discovery and design.

Results

Affinity of CDK2 Inhibitors for Active and Inactive Conformations

The X-ray crystal structures of six CDK2 inhibitors in complex with both monomeric and CDK2/cyclin complexes have been determined, and their structure statistics are summarized in Table S1 (see the Supplemental Data available with this article online). An extensive analysis of these complexes and of other published CDK2 inhibitors bound to monomeric inactive and cyclin activated forms has been carried out to determine the relative binding affinity for inhibitors in both states (Table 1). A total of 17 inactive and 17 active CDK2 inhibitor structures (with 6 novel and 11 from the PDB in both CDK2 conformations) possessing a wide range of potencies in the CDK2/cyclin kinase assays were selected, and the protein/ligand interaction energy was determined. This involved the addition of hydrogens to the PDB structure, followed by a minimization routine keeping all heavy atoms of the protein and ligand fixed, followed by interaction energy calculation. Furthermore, the correlation between the calculated energetics of the complexes and the experimentally derived inhibition constants was examined to ascertain if the monomeric inhibitor complex structure was an accurate reflection of the active CDK2 complex.

This analysis indicates that there is a minimal correlation between inhibitor potency and calculated binding affinity for the inactive enzyme, both for compounds **1–6** (Table 1) and for the PDB ligands in complex with monomeric CDK2 (Figures 1A and 1C). An excellent correlation is observed, however, for the set of cyclin-activated CDK2 inhibitor structures. The relationship between the interaction energies and the IC_{50} values for compounds **1–6** is close to linear, with a correlation coefficient value of 0.85 (Figure 1B). When the data calculated from the PDB structures are included in the analysis, a slightly lower correlation of 0.75 is observed for the active structures (Figure 1D). The new CDK2/cyclin A structures containing pyrimidine-based inhibitor ligands thus further extend and confirm the relationship observed for the diverse ligand group from the PDB. The correlations obtained above are supported by protein/ligand affinity calculations with the LUDI and LigScore1 scoring functions (data not shown), which gave similar results. In addition, the surface area buried upon ligand binding was measured for both sets of structures by calculating the solvent-accessible surface area for the free ligand and protein/ligand complex. These results again demonstrated a close relationship between inhibitor potency and buried surface area in the CDK2/cyclin bound structures, in contrast with the lack of correlation for the monomeric data set (see Supplemental Data).

Given that a strong correlation exists between the enzyme/ligand intermolecular energies and the biochemical ligand inhibition constants in the case of the active CDK2 complex structures (Figures 1B and 1D), it is

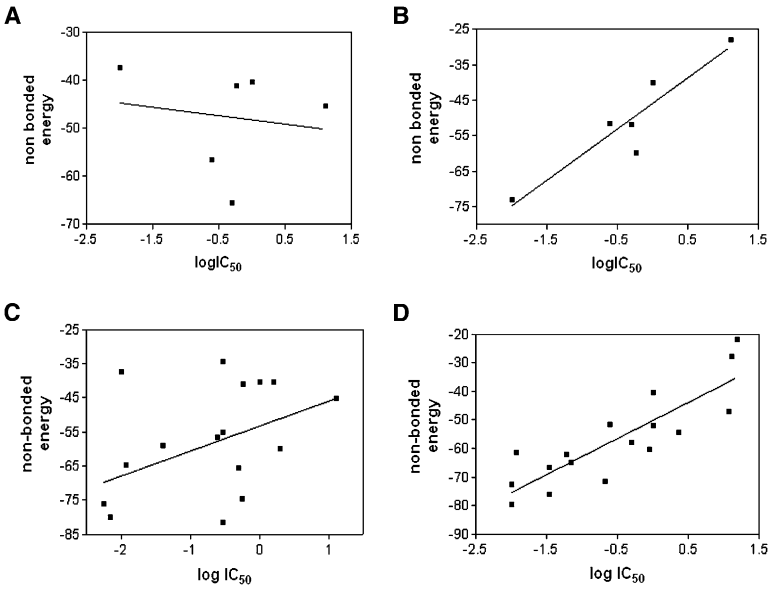

Figure 1. Correlation of Calculated Interaction Energies with Experimental Inhibition Constants

(A–D) Graphs for pyrimidine analogs **1–6** alone ([A], monomeric; [B], active), and including a set of diverse CDK2 inhibitors from the PDB ([C], monomeric; [D], active) in inactive monomeric and active cyclin bound structures.

reasonable to extrapolate values obtained from the crystal structures to determine the relative affinities for the active and inactive forms. Analysis of the data indicates that the ligands NU2058 (−46.9 versus −55.1 kcal/mol) and ATP (−276 versus −672 kcal/mol) would be expected to form tighter complexes with monomeric CDK2.

Extending this affinity analysis for compounds **1–6** shows that the least potent inhibitor **1** has significantly higher affinity for the monomeric species, while the binding energetics predict that of the more potent compounds, **5** and **6** also form tighter complexes with inactive CDK2. Compounds **2** and **4**, on the other hand, bind more avidly to active CDK2/cyclin A, as evidenced by the more favorable energy scores. Compound **3** could be considered to have equal affinity for both active and inactive CDK2 states within the levels of accuracy of the energetics calculation.

In addition to this analysis from CDK2/ligand structures that have been solved in both their inactive and active states, the theoretical binding constants of an additional set of inhibitors were calculated based on their nonbonded energies in the monomeric CDK2 crystal structures extrapolated from the active CDK2 inhibitor correlation (Table 2). This is informative given that no experimental data are available for binding of these inhibitors to the monomeric inactive CDK2. The accuracy of this calculation is valid, since, as shown above in the context of the active enzyme, interaction energies gave a good indication of the experimental inhibition constant (Figures 1B and 1D). These results indicate that 5 out of the 11 CDK2 inhibitors whose affinities were calculated in this way bind with significantly higher affinity to the monomeric enzyme, whereas 4 additional compounds bind with similar potency within the levels of accuracy.

Inhibitor Binding Modes Differ in Monomeric and Cyclin Bound CDK2

To characterize the conformational differences that occur in CDK2 upon activation and to determine the impact of these differences upon protein/ligand interactions, we have solved the structures of six CDK2 inhibitors by X-ray crystallography in both the monomeric and cyclin bound activated complexes. In general, from the CDK2 inhibitor complex structures, the side chains of residues E51, V64, D145, and L148, as well as atoms of residues 10–15 of the Gly-rich loop, adopt different positions in active and inactive CDK2 (Figure 2A). In addition, the catalytic lysine, K33, assumes different conformations in the two structures, and, as a result of activation of CDK2 through cyclin binding and subsequent rotation of the PSTAIRE helix, E51 moves and occupies the space where L148 is found in the inactive CDK2 structure. The largest movement of the residues comprising the ATP binding cleft of CDK2 is that of D145, which moves by 1–2 Å upon activation. Initial analysis of these differences indicates that they would not be expected to have a significant effect on ligand binding, as has been suggested for similar inhibitors bound to both forms of CDK2 [24, 25, 29].

This new data set comprises ligands of varying potencies (Table 1), details the extent of interactions with the ATP binding site, and demonstrates that important variations in the CDK2/ligand interactions and binding mode exist between the two states. These inhibitors are similar, with the exception of **1**, which lacks the phenyl

Table 2. Calculation of Binding Constants for CDK2 Inhibitors in the Monomeric Form

	1H08	1JSV	1JVP	1KE5	1KE6	1OIR	1P2A	1AQ1	1DM2	1E1V	1E1X
NB EGY	−70.9	−60.0	−40.3	−74.7	−76.2	−85.6	−64.8	−79.9	−59.1	−55.1	−34.4
Exp. IC_{50} (μM)	0.300	2.000	1.600	0.560	0.006	0.032	0.012	0.007	0.040	0.300	0.300
Calc. IC_{50} (μM)	0.023	0.170	6.120	0.011	0.009	0.002	0.069	0.004	0.195	0.410	17.890

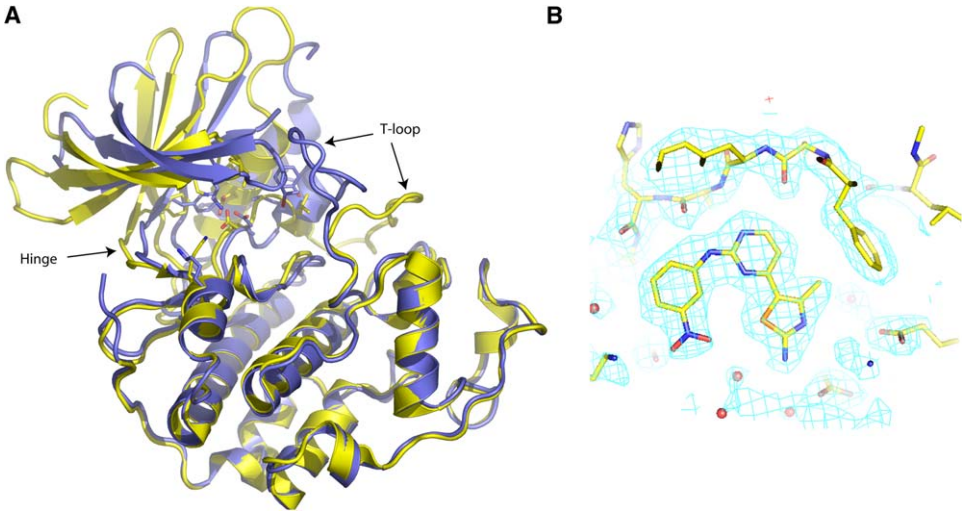

Figure 2. Richardson Diagram of the Overlay of Active and Inactive apo-CDK2

(A) Active apo-CDK2 is shown in yellow; inactive apo-CDK2 is shown in blue. The differences in the orientation of the N and C domains and in the large movement of the T-loop upon cyclin binding can be observed upon overlay of the active and inactive structures from residues 170–285. (B) Electron density difference maps ($2F_o - 1F_c$) in the ATP binding site of the CDK2/cyclin A/4 complex.

substituent on the pyrimidin-2-yl amino group, and **6**, in which the thiazole group is replaced with a [1,2,4]triazol-1-ylmethyl-phenyl system. The CDK2 binding mode of the 2-anilino-4-(thiazol-5-yl)pyrimidine pharmacophore has previously been described (Figure 2B and Figure S1) [28, 30] and includes the following contacts: (1) for the pyrimidine ring: a hydrophobic sandwich between A31 and L134, an H bond between the hinge region residue L83 backbone NH and N1 of the pyrimidine, and an aromatic H-CO interaction between the pyrimidine C6 proton and E81; (2) van der Waals contacts from the aniline ring to the side chain of I10, an H bond between the aniline NH and the L83 carbonyl, and, depending on substitution, varying contacts to Q85, D86, and K89; and, (3) interactions of the thiazole ring with V18, as well as direct contacts of the thiazole 4-methyl with the F80 gatekeeper residue. The thiazole 2-position projects toward the cleft region occupied by the ATP triphosphate.

In order to further investigate the contributions of the protein/ligand interactions to binding in the inactive and active contexts, a detailed contact and energetic analysis for each small-molecule inhibitor was performed (Table 3). Of the new ligand structures presented, the largest observed conformational differences occurred with compound **1** (Figure 3). The NH_2 group of the ligand forms an H bond with the backbone carbonyl of E81 in inactive CDK2. In the active complex, however, the pyrimidine ring flips by 180º, resulting in an interaction of the amino group with the L83 carbonyl. This corresponds to a relative movement of more than 4 Å for both rings of the inhibitor. More favorable interactions are observed with I10 and with K33 in the monomeric CDK2 as a result of close contacts of the pyrimidine and thiazole rings, respectively. In active CDK2, the thiazole system interacts more favorably with F80 (Table 3), packing against its aromatic ring and resulting in displacement of K33 in order to bind similarly to the anilino derivatives (compounds **2**–**5**).

For compounds **2**–**5**, similar binding modes are found in both the active and inactive proteins (Figures 4A and 4B); however, the major differences in the interactions of each segment of the inhibitor are described as follows.

Aniline Region

Significantly different interactions are observed from this part of the inhibitor and the residues of the Gly-rich loop in the activated CDK2. Residues I10, G11, and E12 show variations in energetics between active and inactive CDK2, especially with inhibitors **2**, **4**, and **5** (Table 3). Inhibitors **2** and **4** make significantly more favorable interactions with I10 in the cyclin bound CDK2 due to the closer contacts of the aniline phenyl ring. Also, **4** associates with G11 in the active context through movement of the Gly-rich loop closer to the ligand. Analysis of the contacts with the hinge region and specificity surface (C-lobe loop region of the ATP site) in both CDK2 forms reveals major differences. Firstly, the hinge region undergoes a ligand-induced movement, and this results in significantly different interactions and energetics for some of the inhibitors. In particular, the H84 carbonyl and the Q85 CA shift toward the inhibitor in the active CDK2. This generally results in more favorable interactions of L83 with the anilino function, but it is offset by bad contacts with H84, Q85, and D86 (Table 3) in compounds containing a *para*-substituted aniline (**2**, **3**, and **5**). Secondly, compounds containing bulky *para* substituents (*p*-dimethylamino, **3**; *p*-morpholine, **5**) make detrimental interactions with K89 in active CDK2 compared to the smaller substitutions (*m*-nitro, **4**, and *p*-CF_3, **2**). In particular, the *p*-morpholine of **5** overlaps with K89 and results in movement of the ligand closer to L83, making the H bonding energies with the aniline NH unfavorable. Movement of the ligand as a result of the large substitution forces it to adopt a different conformation distant from the unfavorable site. The consequence of this is relative movement of the thiazole by more than 1 Å.

Table 3. Calculated Intermolecular Energetic Values for CDK2 Residues and Compounds **1**–**6**

CDK2 Residue	1M[a,b]	1C	2M	2C	3M	3C	4M	4C	5M	5C	6M	6C
E8	*−11.0*	*−0.1*	−0.3	−0.2	0.2	0.2	−0.7	−0.5	−0.8	−0.3	0.0	−0.3
I10	*−1.5*	*−0.4*	**−2.7**	**−3.7**	−3.9	−4.1	−2.7	−3.6	−4.2	−4.4	−3.6	−3.0
G11	−0.6	0.0	−0.2	−0.9	−0.1	−0.2	**−0.4**	**−1.5**	−0.3	−0.3	−1.2	−0.6
E12	−1.4	−1.0	−0.1	−0.8	−0.3	0.3	0.6	0.4	−0.4	−1.0	**1.4**	**0.4**
G13	−0.7	−0.7	−0.3	−0.2	−0.5	−0.2	−0.1	−0.8	−0.3	−0.5	**7.4**	**−0.1**
V18	−1.9	−1.5	*−1.5*	*0.3*	−2.0	−2.1	−1.5	−2.1	−1.5	−1.7	*−2.9*	*−1.9*
A31	−0.6	−1.2	−1.0	−0.6	*−1.5*	*−0.5*	−1.3	−1.1	−1.2	−1.6	**−1.8**	**−0.1**
K33	*−5.0*	*−2.4*	**−3.2**	**−4.6**	*−2.5*	*−1.0*	**−3.6**	**−4.8**	*−5.7*	*−4.3*	*−4.2*	*−1.4*
E51	0.2	−0.2	0.1	0.5	0.1	−0.5	**0.2**	**1.4**	0.1	0.9	0.0	−1.1
V64	−0.3	−0.7	−0.8	−0.6	−0.8	−0.6	−0.7	−0.9	−0.8	−0.6	−0.3	−1.0
F80	**−0.8**	**−2.0**	−1.5	−1.6	−1.7	−2.3	−1.3	−2.1	−1.6	−1.4	−2.5	−2.9
E81	**−0.8**	**0.2**	*−2.2*	*−1.0*	−0.2	−1.1	**−0.7**	**−1.9**	**−0.5**	**−1.8**	*−0.3*	*1.8*
F82	−2.5	−2.5	**−1.9**	**−3.8**	−4.1	−3.4	*−3.1*	*−1.9*	−3.5	−3.9	*−3.6*	*−2.2*
L83	*−2.1*	*−1.2*	**2.8**	**−3.1**	**−1.2**	**−2.6**	−3.0	−3.9	**1.6**	**3.0**	**1.1**	**−2.5**
H84	−0.3	−0.4	−0.6	−0.5	*−1.6*	*−0.6*	−1.6	−1.7	*−1.4*	*2.8*	−1.6	−1.5
Q85	−0.1	−0.2	*−1.7*	*0.9*	−2.4	−1.7	−1.6	−1.6	*−2.4*	*0.7*	−1.7	−1.7
D86	**−0.6**	**−2.0**	*−2.7*	*−1.1*	*−2.0*	*−0.9*	−1.1	−1.6	*−2.4*	*−0.9*	−1.8	−0.9
K89	0.9	0.9	**−1.8**	**−2.9**	**1.1**	0.5	**3.6**	**−0.6**	−2.3	−1.7	**1.5**	**−0.6**
Q131	−0.5	−0.3	−0.8	−0.4	−1.1	−0.2	−0.9	−0.6	−0.5	−0.2	*−1.5*	*−0.2*
N132	−0.6	−0.4	−0.7	−0.5	−1.1	−0.3	−0.8	−0.4	−0.7	−0.2	*−0.8*	*1.8*
L134	*−1.0*	*0.2*	*−1.6*	*−0.2*	−1.1	−1.4	−1.7	−2.4	*−1.9*	*0.1*	*−3.5*	*−1.9*
A144	−0.7	−0.6	−1.2	−0.8	−1.2	−0.4	−0.9	−1.3	−0.8	−0.6	−1.7	−0.9
D145	**1.3**	**−0.1**	**6.3**	**0.3**	**4.0**	**−0.4**	**4.7**	**1.1**	**2.0**	**0.6**	−0.4	−0.9
	−45.3	−27.8	−41.1	−60.2	−57.6	−58.1	−37.3	−72.5	−82.0	−40.3	−51.7	−56.7

[a] M and C refer to monomeric (inactive) and cyclin bound (active), respectively.
[b] Values in bold indicate a more favorable interaction with active CDK2; italicized values indicate a more favorable interaction with monomeric CDK2.

Pyrimidine Contacts

The core pyrimidine ring makes similar contacts in both monomeric and cyclin bound CDK2 structures. E81 generally makes a greater contribution to binding of the ligand in the active enzyme, with the exception of **1** and **6**. Close contacts are observed in several of the monomeric-ligand complexes, resulting in offsetting of the enthalpy gain from the CH:O H bond from the pyrimidine ring to the E81 backbone carbonyl.

Thiazole Region

The pocket that accommodates the thiazole systems of the inhibitors includes both hydrophobic (V18, F80) and polar residues (N132, D145). In all structures, F80 makes similar or greater contributions to ligand binding in the active context. Inhibitors **3** and **4** exhibit the most significant favorable change with respect to the cyclin bound CDK2 as a consequence of the movement of F80 to accommodate E51 upon activation. The most dramatic

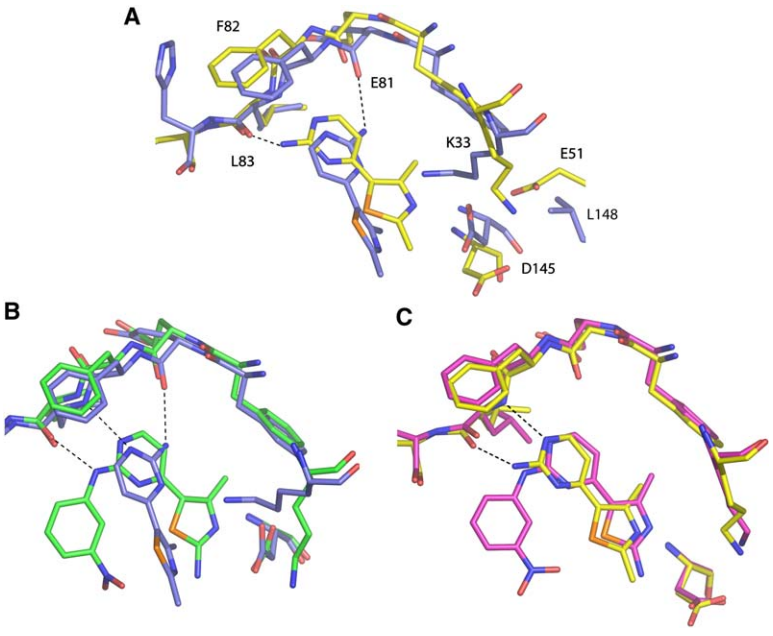

Figure 3. Crystal Structures of Ligands **1** and **4** Bound in Active and Inactive CDK2

(A–C) The overlay shown is residues 77–143 of the same inhibitor (yellow, active; blue, inactive) and with the substituted aniline derivative **4** (yellow) bound in (B) monomeric CDK2 (green) and (C) active (pink) CDK2.

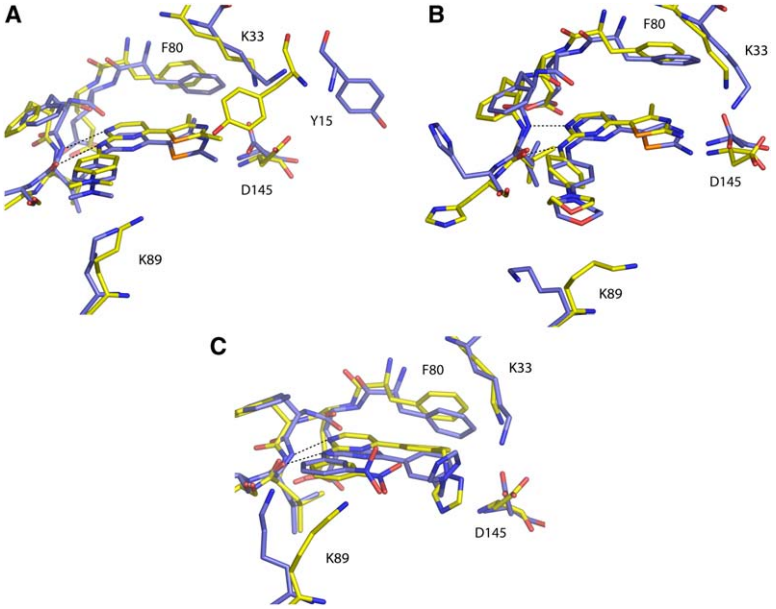

Figure 4. Comparison of the Active and Monomeric CDK2 Binding Modes of Pyrimidine Inhibitors **3**, **5**, and **6**

(A) Inhibitor **3** bound in the ATP binding site of active (yellow) and inactive (blue) CDK2 showing the large shift of Y15 in the active CDK2 structure.

(B) The structures of ligand **5** bound in active (yellow) and inactive (blue) CDK2, overlaid from residues 77–143.

(C) The phenyltriazole group of ligand **6** occupies a different conformation depending on which activation state of CDK2 it is bound to and makes substantially different interactions with the binding site in each context.

changes in this region are involve contributions of D145 to binding of the ligand. With all five thiazole-containing ligand structures of inactive CDK2, interactions with this residue are detrimental to binding (unfavorable energies ranging from +1.3 to +6.3 kcal/mol) as a result of the close proximity of D145 to the inhibitor. Clashes of the thiazol-2-yl-methyl group and the ring nitrogen with the carboxylate are responsible for the unfavorable contributions. Contacts with the side chain of D145 in the active complexes are significantly more favorable, with observed differences resulting in rotation of the carboxylate group about the Cβ-Cγ bond.

Other significant differences observed in the structures of inhibitors **2–5** are in the positions of Y15 and K33. Y15 undergoes a relative change in position in most of the structures; however, only for compound **3** does it move by 10 Å into the ligand binding site in the CDK2/cyclin A structure. For K33, in each of the monomeric complexes the side chain amine projects away from the ligand, whereas, in the active structures, it is much closer to the thiazole ring nitrogen. This movement generally creates a more open pocket in the active CDK2 structures.

Compound **6** (thiazole substituent replaced with a benzyl-triazole) is a unique structure in this series, and of the ligands presented here, it shows the most significant differences in binding to monomeric and active CDK2 (Figure 4C; Table 2) due to the bulkier "head group" extending further into the phosphate binding domain. In the monomeric complex, the triazole ring projects perpendicular from the phenyl toward the Gly-rich loop. In the active CDK2 structure, the triazole shifts by more than 2.5 Å and interacts extensively with D145, an interaction facilitated by the relative shifts of K33 and D145. This is not possible in the monomeric context due to the overlap of the benzyl-triazole group with K33. Another consequence of the enforced alternate triazole conformation in the monomeric enzyme is the relative movement of the phenyl replacement for the thiazole (Figure 4C). This results in effective contacts of the phenyl in the monomeric context with V18 and of the pyrimidine ring with L134 (−1.4 and −1.6 kcal/mol more favorable, respectively).

In order to examine the differences in protein/ligand interactions for CDK2 inhibitor complex structures that have been deposited in the PDB, a data-mining exercise was performed examining the contact information for compounds with a reported IC_{50} against CDK2 of 1 μM or less. The results of the comparison (Table 4) indicate that there are substantial differences in the average number of contacts for residues in the two activation states. Table 4, section A, shows that the PDB ligands in monomeric CDK2 interact more extensively with the side chains of D145 and A144 and the backbone atoms of I10, F82, and L83 (higher ratio of monomeric to active CDK2/ligand contacts). The ligands in complex with CDK2/cyclin A, however, make more contacts with the Gly-rich loop backbone (G11, E12, G13) and also with the side chains of K33, V64, and F82 (Table 4, section B, higher ratio of active to monomeric CDK2/ligand contacts).

Discussion

Implications of Differential CDK2 Inhibitor Binding for Drug Design

The detailed comparison of inhibitors bound to the inactive and active conformations of CDK2 presented here has demonstrated that differences in binding mode can be observed, and that these result in substantially different ligand affinities. The use of the monomeric structural data for ligand design [14, 31, 32] therefore contrasts with that obtained from biological assays since these are based on activated CDK2. Interpretation and evaluation of structural data is therefore often extrapolated from the monomeric to active contexts. Previously, a detailed comparison of diverse ligands bound to both active and inactive forms of CDK2 had not been completed, although some structural information is available [24–26, 29]. In the PDB, there is only one ligand,

Table 4. Comparison of Protein/Ligand Contacts for CDK2 in the Monomeric and Active Forms

	CDK2A		CDK2 Monomer		
A	Number of Contacts	Average	Number of contacts	Average	Average Monomeric/ Active
A144 CB	2	0.1	16	0.9	6.2
F82 C	2	0.1	11	0.6	4.3
D145 OD2	11	0.8	60	3.3	4.2
K89 CA	2	0.1	10	0.6	3.9
F82 CA	5	0.4	22	1.2	3.4
I10 O	3	0.2	12	0.7	3.1
D145 CG	6	0.4	20	1.1	2.6
L83 CA	4	0.3	13	0.7	2.5
F80 CE	4	0.3	11	0.6	2.1
F82 CD	8	0.6	19	1.1	1.8
D145 CB	7	0.5	15	0.8	1.7
Q131 O	8	0.6	16	0.9	1.6
B					Average Active/ Monomeric
E12 N	10	0.7	1	0.1	12.9
G11 C	10	0.7	2	0.1	7.1
E12 C	11	0.8	3	0.2	4.7
G13 N	9	0.6	3	0.2	3.9
D145 N	9	0.6	3	0.2	3.9
G12 O	9	0.6	3	0.2	3.9
G13 CA	14	1.0	7	0.4	2.6
Q85 CA	34	2.4	19	1.1	2.3
N132 OD1	15	1.1	9	0.5	2.1
G11 CA	8	0.6	5	0.3	2.1
F82 CZ	9	0.6	6	0.3	1.9
F82 CE	25	1.8	17	0.9	1.9
D86 N	19	1.4	13	0.7	1.9
K33 CE	10	0.7	8	0.4	1.6
K33 NZ	10	0.7	8	0.4	1.6
V64 CG	23	0.8	18	0.5	1.6
F80 CB	24	1.7	20	1.1	1.5
K89 CD	19	1.4	17	0.9	1.4
F80 CD	29	2.1	26	1.4	1.4
I10 CG2	57	2.0	55	1.5	1.3

Sections A and B indicate the CDK2 atom with the higher average number of contacts in the monomeric and active forms, respectively.

NU2058, for which a complex crystal structure has been solved with both CDK2 and CDK2/cyclin A. Indirubin-5-sulfonate has previously been shown to bind in similar conformations in monomeric and binary CDK2 and makes common interactions with both states [26]. One of the residues that shifts most significantly upon activation, D145, adopts a rotamer state more similar to that in the monomeric structure, although there is an ~1 Å shift in the position of this side chain. Further direct comparisons of this ligand bound to monomeric and active CDK2 were not possible since only one set of coordinates was deposited in the PDB.

The new data presented therefore extend and further illustrate that significant differences in protein/ligand interactions are observed between the two states of CDK2, and, therefore, due care should be taken in the structure-guided discovery and design of kinase inhibitors. These data demonstrate that diverse CDK2 pharmacophores can make quite different interactions in monomeric structures routinely used for informing ligand design when compared to the active enzyme. This is especially true for inhibitors **1** and **6**, in which interpretations from the binary ligand complex would quite possibly be misleading (Figures 3 and 4C). Compound **1** is the most dramatic example, and, in this case, the low-affinity inhibitor (an initial screening hit) undergoes a 180° rotation in binding mode (Figures 3A–3C). Structure-based design with the monomeric information could result in the wrong analogs being synthesized in the early stages of lead optimization against activated CDK2, with potentially detrimental consequences.

For the inhibitors studied that have a similar binding mode in both the monomeric and cyclin bound CDK2, the ligand contacts with the Gly-rich loop and the side chains of K33 and D145 vary significantly. From observations of the unliganded structures of CDK2, rotation of the PSTAIRE helix upon cyclin binding results in movement of E51 into, and L148 out of, the ATP binding site. As a result, the ion-pairing interaction between K33 and D145 is broken, and the latter residue projects away from the cleft, while K33 now forms a new salt bridge with E51. These changes result in differing interactions of the inhibitor with K33 and D145 in the novel active ligand structures presented here and more favorable contributions of D145 to inhibitor binding.

This is illustrated most dramatically in the structures of inhibitor **6**. This analog displays significantly different interactions of the benzyl-triazole moiety with the ATP pocket (Figure 4C). The triazole conformation of the CDK2/cyclin A bound ligand cannot be accommodated with the positions of K33 and D145 observed in the monomeric enzyme, and it is displaced toward the Gly-rich loop. The observed displacement leads to a different set of interactions of the triazole and more optimal hydrophobic contacts of the inhibitor as a whole, with the energetic analysis showing that it binds more tightly to inactive CDK2. The differences in binding mode suggest that structure-guided optimization against cyclin-activated CDK2, with crystallography of the inactive enzyme, could lead to erroneous interpretations of structural data. These observed differences for inhibitor **6** are likely to be true for all CDK2 ligands that interact with the phosphate binding region.

Even for the case in which ligands bind with similar conformations in both contexts, the inactive CDK2 structure may still provide inadequate or misleading information. Analysis of the monomeric crystal structure of inhibitor **4** did not adequately explain the structure-activity relationship that had been determined by using an in vitro kinase assay. In particular, replacement of the 2-methyl group of the thiazole ring with an amino function resulted in a 100-fold potency enhancement [27], although the inactive crystal structure of this analog did not reveal a favorable interaction of the amino group. Solution of the CDK2/cyclin A/**4** complex showed that the ligand NH_2 donates an H bond to the D145 carboxylate; therefore, the position of this residue in inactive CDK2 did not accurately resolve the structure-activity relationship of the inhibitor described experimentally. This is further illustrated by comparing the structures of **5**, for which a significant movement of the thiazole ring occurs. Unfavorable interactions of the aniline substitution and the resulting displacement of the thiazole system leads to inaccessibility of the thiazole 2-amino group on the thiazole for H bond formation to D145.

In comparing the structures of compounds **1–6**, significant differences were observed for Y15; however, even in the case of the largest movement of this residue (compound **3**, Figure 4A), a minimal contribution to inhibitor binding occurred (Table 3). The possibility that this residue may impact structure-guided design should therefore be considered in some contexts.

The observations made on the basis of the six inhibitors whose crystal structures were solved in both the inactive and activated CDK2 forms have been supported by the analysis of protein/ligand interactions in the ligands obtained from the PDB. Through the contact analysis method, significant general differences have been described (Table 4), indicating that the contact profiles obtained in the pyrimidine comparison are not specific for this pharmacophore. The ligands of the PDB inhibitor set make predominant contacts with the Gly-rich loop in the active enzyme, consistent with the different conformation of this region of CDK2 and with the observations described for our compounds. Also, as indicated in the pyrimidine inhibitor structures, the PDB ligands in the inactive CDK2 contain multiple contacts with the D145 side chain. Many of these contacts are overlapping and also are not observed in the active complexes. Also, consistent with the new ligands presented are the different interactions with the hinge region backbone in both contexts and the contacts observed with I10. The marked increase in contacts to V64 in the active structures in comparison to the monomeric structure is surprising, as this was not observed with our pyrimidine inhibitors, although this may be the result of unique interactions of this series.

The differences in ligand binding mode and energetics described in the two forms of CDK2 are mainly caused by conformational differences in the binding site. As has been shown, this depends on the size and complementarity of the inhibitor and the way in which the basic pharmacophore template of the inhibitor is functionalized. As we have observed, the smaller ligand **1** (Figure 3A) more easily adopts a different conformation in order to compensate for the differences in the binding site between monomeric and cyclin bound CDK2. Larger ligands cannot easily adopt alternate conformations since these may result in more extensive, unfavorable interactions in the binding site (Figures 3B and 3C). In addition, unfavorable side chain conformations that may occur would not override favorable ligand binding enthalpies; however, they will decrease the overall affinity of the ligand in either context. In the pyrimidine series, this applies to ligands with a substituted aniline nitrogen (compounds **2–6**) since adjustment of the conformation of the inhibitor would result in atom overlap with H84, Q85, and K89. These ligands could not adopt similar conformations compared to **1** in the monomeric CDK2, as this would result in steric clashes with atoms of F80 and E81 (Figure 3B). These observations thus further underline the necessity to compare liganded structures of CDK2 in both inactive and active contexts. The application of these results in drug discovery and optimization therefore indicates that caution should be exercised in the context in which structural information for an inhibitor is obtained. Our results show that if active CDK2 is used for in vitro screening, then structural information should be interpreted accurately on the basis of these data. Although monomeric CDK2 structures require less effort and are generally obtained to higher resolution, it would be expedient to obtain at least one active ligand complex structure in order to confirm and further inform the structure-activity relationship observed from the CDK2/cyclin kinase assay.

Consequences of Structural and Affinity Differences for In Silico Screening

Due to the observed differences in ligand binding to active CDK2 complexes, the use of monomeric structures as templates for high-throughput docking may not produce the best results. Although virtual screening can undoubtedly lead to enrichment over random screening methods [28], further improvements in hit rates should be obtained though inclusion of an active CDK2 structure in the docking stage. Even in the situation in which a ligand binds similarly in both structural forms (Figures 4A and 4B), the ligand would probably not be scored correctly, since, as shown, measured interaction energies do not correlate with binding in the monomeric protein. Docked poses would therefore likely be incorrectly ranked in the inactive CDK2, resulting in inaccurate predictions of small-molecule inhibitor binding. If in silico screening is to be performed on the inactive CDK2, our data suggest that the best results would be obtained only if experimental binding constants were determined with an assay based on the monomeric kinase.

A recent study from this laboratory examined the influence of CDK2 structure on the extent of successful reproduction of crystallographic binding mode by high-throughput docking programs [33]. The conclusions drawn were that the positioning of side chains, and the volume of the binding site, are the critical factors in determining how many ligands dock with the correct pose, and that use of the activated CDK2 structures results in the most success in this regard. This study confirms the observations that the positions of the side chains of K33, F80, K89, and D145 are important, as is that of the Gly-rich loop.

Prospects for Selectively Targeting Inactive CDK Conformations

The results presented here also have implications for inhibitor design aimed at preferentially targeting kinase structures that are in the inactive form. Recently, several complex crystal structures of protein kinase inhibitors have demonstrated that predominant binding to inactive conformations can be crucial to their mode of inhibition [34]. Binding in these instances produced highly selective ligands, since inactive kinase structures are often unique in terms of their interactions with the ligand in comparison to the active ones. The results presented here from the energetic analysis of CDK2 inhibitors in both their binary and ternary complexes suggest that it is feasible to generate potent CDK2 inhibitors that bind with significantly higher affinity to the inactive conformation of this enzyme. Some inhibitors make tight interactions with D145 and therefore stabilize the inactive conformation. A positive outcome of this is that ligands that have greater specificity for the inactive CDK2 can, in principle, be designed. Energetic analysis showed that the affinity of ATP for the inactive enzyme is considerably greater than that observed for the cyclin-complexed

CDK2. The weaker binding of ATP in the active form could be explained by the fact that exposure of the γ-PO_4 (buried in the monomeric structure) is required for catalytic phosphotransfer to occur. Consequently, many interactions with the γ- and β-phosphates observed in the monomeric structure are not present in the active form. Analysis of the ATP bound structures in which the γ-phosphate required for catalysis is buried suggests that further targeting the phosphate binding region could result in highly selective binding to the inactive CDK2 conformation.

We have shown previously that CDK2 inhibitors induce significant disordering of the T-loop when bound to the monomeric protein [28]. Displacement of K33 from the salt bridge with D145 results in movement of the Gly-rich loop and subsequent activation loop disordering. In the context of these results, it is conceivable that where inhibitors bind tightly to the monomeric CDK2 and sequester it in this form, they could prevent activation by the cyclin molecule in a particular cell cycle compartment. Specificity of inhibitors for the inactive CDK2 conformation should also result in a greater selectivity for this kinase as a target in the cellular context, as the ATP binding site would be in a more distinct conformation, although this would not be reflected in the in vitro kinase assay. Competitive binding assays with fluorescently labeled inhibitors that allow quantification of direct binding to protein kinases could be used to determine affinity for both active and inactive conformations of CDK2. Selectivity for monomeric CDK2 would also be applicable to inhibiting any cyclin-independent kinase activity associated with phosphorylated protein [21]. The significant level of kinase activity of the phosphorylated monomeric protein is likely to be biologically relevant given that the CDKs are present throughout the cell cycle and are only transiently activated by cyclins. The results obtained in this study thus warrant additional experiments comparing binding to inactive and active CDK2 with the potential aim of selectively targeting these conformations.

Significance

Through comparison of a number of new CDK2 inhibitor structures we have demonstrated that ligand-protein kinase interactions and conformations vary substantially between the active and inactive forms. Energetic analysis of these inhibitors bound to both monomeric and binary CDK2 forms has revealed details of the differences in inhibitor binding mode and induced protein changes. These differences were additionally confirmed through extraction of CDK2 inhibitor protein-ligand contact information from a selection of potent inhibitors whose structures were previously solved in either the monomeric or active forms. Calculation of the intermolecular binding energies from the crystal structures has demonstrated that while the monomeric CDK2 ligand complexes are not reflective of the experimentally obtained inhibition constants, the CDK2/cyclin A bound inhibitor structures correlate accurately with the in vitro assay data. These results have significant implications for structure-based ligand discovery and design in that, if the key differences in interactions are accounted for with in silico screening and inhibitor optimization, then an enhancement in success criteria should be obtained. The analysis also indicates that ligands can potentially be designed selectively to target the inactive conformation of CDKs, and that this may result in more selective ligands being obtained.

Experimental Procedures

Human recombinant CDK2 and human recombinant cyclin A2 (fragment encompassing residues 173–432) were expressed, purified, and crystallized as previously described [28, 35]. Biochemical assays were carried out as reported previously [36, 37].

Structure Determination

Data were collected at the Daresbury (UK) and Grenoble (France) synchrotron facilities by using an ADSC Quantum4 CCD detector and home with a Raxis IV++ image plate (Rigaku). Data processing was carried out with the programs DENZO and SCALEPACK [38], or the d*TREK software suite [39] or MOSFLM [40] and SCALA [41] from the CCP4 program suite [42]. Data often showed signs of crystal radiation damage. The structures were solved by molecular replacement with MOLREP [43] and PDB entries 1PW2 and 1OKV as the search models for CDK2 and CDK2/cyclin A, respectively. ARP/wARP [44] was used for initial density interpretation and the addition of water molecules. REFMAC [43] was used for structural refinement. A number of rounds of refinement and model building with the program Quanta (Accelrys, San Diego, CA) were carried out.

Computational Chemistry

Calculation of protein/ligand interaction energies between inhibitor and CDK2 or the CDK2/cyclin A complex was performed by using the AFFINITY module after addition of hydrogens and 200 steps of steepest-descent minimization with the program DISCOVER of the modeling package InsightII (Accelrys). As heavy atoms of the protein and ligand were fixed, the minimization was performed to relieve high energies as a result of hydrogen addition to the crystal structures. Affinity measures the van der Waals and electrostatic intermolecular energies. The ligscore1 and LUDI scoring functions of the Cerius2 program (Accelrys) were also used in order to determine inhibitor binding energy. The analysis of CDK2 inhibitor intermolecular contacts from the PDB (Table 4) was carried out by extracting all protein/ligand contacts less than 4 Å on an atomic basis by using the program Quanta (Accelrys). Structures of monomeric and active CDK2 structures from the PDB having an IC_{50} value of less than 1 μM were used for this analysis. For each set of monomeric and active structures, the total number of contacts for each protein atom within the distance cutoff was generated and subsequently averaged over all structures. In order to facilitate comparison between monomeric and active liganded structures, tables were sorted according to the total number of contacts per atom and the number of contacts averaged over all of the structures in each category.

Synthesis

Preparations of compounds **1–5** were previously described [27].

3-Nitro-phenyl-[4-(3-[1,2,4]triazol-1-ylmethyl-phenyl)-pyrimidin-2-yl]-amine

A mixture of 3-dimethylamino-1-(3-[1,2,4]triazol-1-ylmethyl-phenyl)-propenone and 1.5 molar equivalents each of 3-nitro-phenyl guanidine nitrate and NaOH in 2-methoxylethanol was heated at 125ºC for 20 hr. The solvent was evaporated, and the residue was purified by silica gel chromatography by using elution with EtOAc and then EtOAc/MeOH (10:1) to afford the title compound as a yellow solid (yield 50%). Anal RP-HPLC (Vydac 218TP54 250 × 4.6 mm columns, linear gradient elution with H_2O/MeCN systems containing 0.1% CF_3COOH at a flow rate of 1 ml/min): t_R = 17 min (0%–60% MeCN, purity 99%; ^{1}H-NMR (500 MHz, DMSO-d_6): δ 5.54 (s, 2H, CH_2), 7.43 (d, 1H, J = 8.0 Hz, Ph-H), 7.51 (d, 1H, J = 5.0 Hz, pyrimidine-H), 7.54 (t, 1H, J = 8.0 Hz, Ph-H), 7.58 (t, 1H, J = 8.0 Hz, Ph-H), 7.81 (d, 1H, J = 8.0 Hz, Ph-H), 7.98 (s, 1H, Ph-H), 8.07 (d, 1H, J = 8.0 Hz, Ph-H), 8.15 (d, 1H, J = 8.0 Hz, Ph-H), 8.21 (s, 1H, Ph-H), 8.65 (d, 1H, J = 5.0 Hz, pyrimidine-H), 8.70 (s, 1H, triazol-H), 9.11 (s, 1H, triazol-H),

10.27 (s, 1H, NH). MS (ESI$^+$) *m/z* 374.4 $[M+H]^+$, $C_{19}H_{15}N_7O_2$ requires 373.37.

3-Dimethylamino-1-(3-[1,2,4]triazol-1-ylmethyl-phenyl)-propenone

A solution of 1-*m*-tolyl-ethanone (5.0 g, 37.3 mmol) in anh. MeCN (45 ml) was treated with *N*-bromosuccinimide (6.63 g, 37.3 mmol) and benzoyl peroxide (9.02 g, 37.3 mmol). The reaction mixture was heated at 80ºC for 6 hr. Upon cooling, the mixture was concentrated, and the resulting syrup was dissolved in Et_2O and treated with $NaHCO_3$. The ethereal layer was washed with brine and dried on $MgSO_4$. The solvent was evaporated, and the resulting residue was purified by silica gel chromatography (heptane/EtOAc 12:1–3:1) to afford 1-(3-bromomethyl-phenyl)-ethanone (5.5 g, 69%). ^{1}H-NMR ($CDCl_3$): δ 2.54 (s, 3H, CH_3), 4.45 (s, 2H, CH_2), 7.38 (t, 1H, *J* = 8.0 Hz, Ph-H), 7.52 (d, 1H, *J* = 8.0 Hz, Ph-H), 7.81 (d, 1H, *J* = 8.0 Hz, Ph-H), 7.90 (s, 1H, Ph-H).

1*H*-[1,2,4]triazole (0.15 g, 2.25 mmol) in anh. DMF (8 ml) was cooled on an ice bath and treated with Cs_2CO_3 (0.67 g, 2.07 mmol). After stirring for 30 min, 1-(3-bromomethyl-phenyl)-ethanone (0.4 g, 1.88 mmol) was added. The reaction mixture was warmed to room temperature and was stirred for 20 hr. Ice water was added, and the mixture was extracted with Et_2O. The combined extracts were washed with brine and dried on $MgSO_4$. The solvent was evaporated, and the residue was purified by silica gel chromatography by using heptane/EtOAc (12:1–3:1) to afford 1-(3-[1,2,4]triazol-1-ylmethyl-phenyl)-ethanone (0.23 g, 60%). ^{1}H-NMR ($CDCl_3$) δ: 2.58 (s, 3H, CH_3), 5.39 (s, 2H, CH_2), 7.45 (d, 1H, *J* = 7.5 Hz, Ph-H), 7.47 (t, 1H, *J* = 7.5 Hz, Ph-H), 7.87 (s, 1H, Ph-H), 7.92 (d, 1H, *J* = 7.5 Hz, Ph-H), 7.97 (s, 1H, triazol-H), 8.11 (s, 1H, triazol-H).

An aliquot of this material (0.10 g, 0.50 mmol) was treated with *N,N*-dimethyl formamide dimethylacetal (1 ml, 8.39 mmol) at 100ºC for 7 hr. Upon cooling, the reaction mixture was concentrated, and the resulting residue was purified by silica chromatography by using heptane/EtOAc (3:1–1:10) to afford 3-dimethylamino-1-(3-[1,2,4]triazol-1-ylmethyl-phenyl)-propenone as a yellow solid (80% yield). ^{1}H-NMR ($CDCl_3$) δ: 2.89 (s, 3H, CH_3), 3.12 (s, 3H, CH_3), 5.45 (s, 2H, CH_2), 5.76 (d, 1H, *J* = 12.5 Hz, CH), 7.35 (d, 1H, *J* = 8.0 Hz, Ph-H), 7.40 (d, 1H, *J* = 8.0 Hz, Ph-H), 7.70 (d, 1H, *J* = 12.5 Hz, CH), 7.79 (s, 1H, Ph-H), 7.82 (d, 1H, *J* = 8.0 Hz, Ph-H). 7.97 (s, 1H, triazol-H), 8.67 (s, 1H, triazol-H).

Supplemental Data

Supplemental Data including Table S1 (crystallographic data and statistics) and Figure S1 (schematic representation of the CDK2 binding mode of compounds **2–5**) are available at http://www.chembiol.com/cgi/content/full/13/2/201/DC1/.

Acknowledgments

We would like to thank Dr. David Blake and many colleagues at Cyclacel for their contributions. We thank Professors Eldrige Buultjens and Nikolai Zhelev at the University of Abertay, Dundee for their support of S.R.P. We would also like to acknowledge the staff of beamlines ID 14.1 and 14.2 at the European Synchrotron Radiation Facility for their assistance as well as Pierre Rizkallah at Synchrotron Radiation Source Daresbury for the data collection for the CDK2/cyclin A/6 complex.

Received: September 12, 2005
Revised: November 18, 2005
Accepted: November 18, 2005
Published: February 24, 2006

References

1. Sausville, E.A. (2002). Complexities in the development of cyclin-dependent kinase inhibitor drugs. Trends Mol. Med. *8*, S32–S37.
2. Ortega, S., Malumbres, M., and Barbacid, M. (2002). Cell cycle and cancer: the G1 restriction point and the G1/S transition. Curr. Genomics *3*, 245–263.
3. Tetsu, O., and McCormick, F. (2003). Proliferation of cancer cells despite CDK2 inhibition. Cancer Cell *3*, 233–245.
4. Grim, J.E., and Clurman, B.E. (2003). Cycling without CDK2? Trends Cell Biol. *13*, 396–399.
5. Blagosklonny, M.V. (2004). Do cells need CDK2 and Bcr-Abl? Cell Death Differ. *11*, 249–251.
6. Fischer, P.M. (2004). The use of CDK inhibitors in oncology: a pharmaceutical perspective. Cell Cycle *3*, 742–746.
7. Kaldis, P. (1999). The cdk-activating kinase (CAK): from yeast to mammals. Cell. Mol. Life Sci. *55*, 284–296.
8. Napolitano, G., Majello, B., and Lania, L. (2002). Role of cyclinT/Cdk9 complex in basal and regulated transcription (Review). Int. J. Oncol. *21*, 171–177.
9. Oelgeschlager, T. (2002). Regulation of RNA polymerase II activity by CTD phosphorylation and cell cycle control. J. Cell. Physiol. *190*, 160–169.
10. Agbottah, E., de La Fuente, C., Nekhai, S., Barnett, A., Gianella-Borradori, A., Pumfery, A., and Kashanchi, F. (2005). Antiviral activity of CYC202 in HIV-1-infected cells. J. Biol. Chem. *280*, 3029–3042.
11. Koumenis, C., and Giaccia, A. (1997). Transformed cells require continuous activity of RNA polymerase II to resist oncogene-induced apoptosis. Mol. Cell. Biol. *17*, 7306–7316.
12. Ljungman, M., and Lane, D.P. (2004). Opinion: transcription - guarding the genome by sensing DNA damage. Nat. Rev. Cancer *4*, 727–737.
13. Huwe, A., Mazitschek, R., and Giannis, A. (2003). Small molecules as inhibitors of cyclin-dependent kinases. Angew. Chem. Int. Ed. Engl. *42*, 2122–2138.
14. Fischer, P.M., Endicott, J., and Meijer, L. (2003). Cyclin-dependent kinase inhibitors. In Progress in Cell Cycle Research, Volume 5, L. Meijer, A. Jézéquel, and M. Roberge, eds. (Roscoff, France: Editions de la Station Biologique de Roscoff), pp. 235–248.
15. Dai, Y., and Grant, S. (2003). Cyclin-dependent kinase inhibitors. Curr. Opin. Pharmacol. *3*, 362–370.
16. Noble, M.E., Endicott, J.A., and Johnson, L.N. (2004). Protein kinase inhibitors: insights into drug design from structure. Science *303*, 1800–1805.
17. Jeffrey, P.D., Russo, A.A., Polyak, K., Gibbs, E., Hurwitz, J., Massague, J., and Pavletich, N.P. (1995). Mechanism of CDK activation revealed by the structure of a cyclinA-CDK2 complex. Nature *376*, 313–320.
18. Honda, R., Lowe, E.D., Dubinina, E., Skamnaki, V., Cook, A., Brown, N.R., and Johnson, L.N. (2005). The structure of cyclin E1/CDK2: implications for CDK2 activation and CDK2-independent roles. EMBO J. *24*, 452–463.
19. Morris, M.C., Gondeau, C., Tainer, J.A., and Divita, G. (2002). Kinetic mechanism of activation of the CDK2/cyclin A complex. Key role of the C-lobe of the Cdk. J. Biol. Chem. *277*, 23847–23853.
20. Connell-Crowley, L., Solomon, M.J., Wei, N., and Harper, J.W. (1993). Phosphorylation independent activation of human cyclin-dependent kinase 2 by cyclin A in vitro. Mol. Biol. Cell *4*, 79–92.
21. Brown, N.R., Noble, M.E., Lawrie, A.M., Morris, M.C., Tunnah, P., Divita, G., Johnson, L.N., and Endicott, J.A. (1999). Effects of phosphorylation of threonine 160 on cyclin-dependent kinase 2 structure and activity. J. Biol. Chem. *274*, 8746–8756.
22. De Bondt, H.L., Rosenblatt, J., Jancarik, J., Jones, H.D., Morgan, D.O., and Kim, S.H. (1993). Crystal structure of cyclin-dependent kinase 2. Nature *363*, 595–602.
23. Heitz, F., Morris, M.C., Fesquet, D., Cavadore, J.-C., Doree, M., and Divita, G. (1997). Interactions of cyclins with cyclin-dependent kinases: a common interactive mechanism. Biochemistry *36*, 4995–5003.
24. Arris, C.E., Boyle, F.T., Calvert, A.H., Curtin, N.J., Endicott, J.A., Garman, E.F., Gibson, A.E., Golding, B.T., Grant, S., Griffin, R.J., et al. (2000). Identification of novel purine and pyrimidine cyclin-dependent kinase inhibitors with distinct molecular interactions and tumor cell growth inhibition profiles. J. Med. Chem. *43*, 2797–2804.
25. Davis, S.T., Benson, B.G., Bramson, H.N., Chapman, D.E., Dickerson, S.H., Dold, K.M., Eberwein, D.J., Edelstein, M., Frye, S.V., Gampe, R.T., Jr., et al. (2001). Prevention of chemotherapy-induced alopecia in rats by CDK inhibitors. Science *291*, 134–137.

26. Davies, T.G., Tunnah, P., Meijer, L., Marko, D., Eisenbrand, G., Endicott, J.A., and Noble, M.E. (2001). Inhibitor binding to active and inactive CDK2: the crystal structure of CDK2-cyclin A/indirubin-5-sulphonate. Structure *9*, 389–397.

27. Wang, S., Meades, C., Wood, G., Osnowski, A., Anderson, S., Yuill, R., Thomas, M., Mezna, M., Jackson, W., Midgley, C., et al. (2004). 2-Anilino-4-(thiazol-5-yl)pyrimidine CDK inhibitors: synthesis, SAR analysis, X-ray crystallography, and biological activity. J. Med. Chem. *47*, 1662–1675.

28. Wu, S.Y., McNae, I., Kontopidis, G., McClue, S.J., McInnes, C., Stewart, K.J., Wang, S., Zheleva, D.I., Marriage, H., Lane, D.P., et al. (2003). Discovery of a novel family of CDK inhibitors with the program LIDAEUS: structural basis for ligand-induced disordering of the activation loop. Structure *11*, 399–410.

29. Davies, T.G., Bentley, J., Arris, C.E., Boyle, F.T., Curtin, N.J., Endicott, J.A., Gibson, A.E., Golding, B.T., Griffin, R.J., Hardcastle, I.R., et al. (2002). Structure-based design of a potent purine-based cyclin-dependent kinase inhibitor. Nat. Struct. Biol. *9*, 745–749.

30. Wang, S., Wood, G., Meades, C., Griffiths, G., Midgley, C., McNae, I., McInnes, C., Anderson, S., Jackson, W., Mezna, M., et al. (2004). Synthesis and biological activity of 2-anilino-4-(1H-pyrrol-3-yl) pyrimidine CDK inhibitors. Bioorg. Med. Chem. Lett. *14*, 4237–4240.

31. Dreyer, M.K., Borcherding, D.R., Dumont, D.A., Peet, N.P., Tsay, J.T., Wright, P.S., Bitonti, A.J., Shen, J., and Kim, S.-H. (2001). Crystal structure of human cyclin-dependent kinase 2 in complex with the adenine-derived inhibitor H717. J. Med. Chem. *44*, 524–530.

32. Davies, T.G., Pratt, D.J., Endicott, J.A., Johnson, L.N., and Noble, M.E. (2002). Structure-based design of cyclin-dependent kinase inhibitors. Pharmacol. Ther. *93*, 125–133.

33. Thomas, M.P., McInnes, C., and Fischer, P.M. (2006). Protein structures in virtual screening: a case study with CDK2. J. Med. Chem. *49*, 92–104.

34. Schindler, T., Bornmann, W., Pellicena, P., Miller, W.T., Clarkson, B., and Kuriyan, J. (2000). Structural mechanism for STI-571 inhibition of abelson tyrosine kinase. Science *289*, 1938–1942.

35. Kontopidis, G., Andrews, M.J.I., McInnes, C., Cowan, A., Powers, H., Innes, L., Plater, A., Griffiths, G., Paterson, D., Zheleva, D.I., et al. (2003). Insights into cyclin groove recognition: complex crystal structures and inhibitor design through ligand exchange. Structure *11*, 1537–1546.

36. McInnes, C., Andrews, M.J., Zheleva, D.I., Lane, D.P., and Fischer, P.M. (2003). Peptidomimetic design of CDK inhibitors targeting the recruitment site of the cyclin subunit. Curr. Med. Chem. Anti-Canc. Agents *3*, 57–69.

37. Zheleva, D.I., McInnes, C., Gavine, A.L., Zhelev, N.Z., Fischer, P.M., and Lane, D.P. (2002). Highly potent p21(WAF1)-derived peptide inhibitors of CDK-mediated pRb phosphorylation: delineation and structural insight into their interactions with cyclin A. J. Pept. Res. *60*, 257–270.

38. Otwinowski, Z., and Minor, W. (1997). Processing of X-ray diffraction data collected in oscillation mode. Methods Enzymol. *276*, 307–326.

39. Pflugrath, J. (1999). The finer things in X-ray diffraction data collection. Acta Crystallogr. D Biol. Crystallogr. *55*, 1718–1725.

40. Leslie, A.G.W. (1992). Recent changes to the MOSFLM package for processing film and image plate data. In Joint CCP4 + ESF-EAMCB Newsletter on Protein Crystallography, Volume 26.

41. Evans, P.R. (1993). Data reduction. In Proceedings of CCP4 Study Weekend on Data Collection & Processing, pp. 114–122.

42. CCP4 (Collaborative Computational Project, Number 4) (1994). The CCP4 suite: programs for protein crystallography. Acta Crystallogr. D Biol. Crystallogr. *50*, 760–763.

43. Murshudov, G.N., Vagin, A.A., and Dodson, E.J. (1997). Refinement of macromolecular structures by the maximum-likelihood method. Acta Crystallogr. D Biol. Crystallogr. *53*, 240–255.

44. Lamzin, V.S., and Wilson, K.S. (1997). Automated refinement for protein crystallography. Methods Enzymol. *277*, 269–305.

Accession Numbers

Structures have been deposited in the Protein Data Bank under accession codes 2C5O, 2C5V, 2C5N, 2C5P, 2C5T, and 2C5Y for the CDK2/CA complexes with inhibitors **1–6**, respectively, and 2C5Y for the CDK2 complex with **6**.